Bioactive Materials 30 (2023) 62–72

Contents lists available at ScienceDirect

Bioactive Materials

journal homepage: www.keaipublishing.com/en/journals/bioactive-materials

Complex coacervate-derived hydrogel with asymmetric and reversible wet bioadhesion for preventing UV light-induced morbidities

Xin Peng [a,1], Yuan Li [b,1], Menghui Liu [a,1], Zhuo Li [c], Xuemei Wang [c], Kunyu Zhang [c,**], Xin Zhao [d,***], Gang Li [b,****], Liming Bian [c,*]

[a] Guangdong Provincial Engineering Research Center of Molecular Imaging, The Fifth Affiliated Hospital, Sun Yat-sen University, Zhuhai, 519000, China
[b] Department of Orthopaedics & Traumatology, Stem Cells and Regenerative Medicine Laboratory, Li Ka Shing Institute of Health Sciences, The Chinese University of Hong Kong, Prince of Wales Hospital, Shatin, 999077, Hong Kong Special Administrative Region
[c] School of Biomedical Sciences and Engineering, Guangzhou International Campus, National Engineering Research Center for Tissue Restoration and Reconstruction, Guangdong Provincial Key Laboratory of Biomedical Engineering, Key Laboratory of Biomedical Materials and Engineering of the Ministry of Education, South China University of Technology, Guangzhou, 510006, PR China
[d] Department of Biomedical Engineering, The Hong Kong Polytechnic University, Hong Kong

ARTICLE INFO

Keywords:
Adhesive hydrogel
Coacervate
Asymmetric adhesion
Reversible adhesion

ABSTRACT

Protecting the skin from UV light irradiation in wet and underwater environments is challenging due to the weak adhesion of existing sunscreen materials but highly desired. Herein we report a polyethyleneimine/thioctic acid/titanium dioxide (PEI/TA/TiO_2) coacervate-derived hydrogel with robust, asymmetric, and reversible wet bioadhesion and effective UV-light-shielding ability. The PEI/TA/TiO_2 complex coacervate can be easily obtained by mixing a PEI solution and TA/TiO_2 powder. The fluid PEI/TA/TiO_2 coacervate deposited on wet skin can spread into surface irregularities and subsequently transform into a hydrogel with increased cohesion, thereby establishing interdigitated contact and adhesion between the bottom surface and skin. Meanwhile, the functional groups between the skin and hydrogel can form physical interactions to further enhance bioadhesion, whereas the limited movement of amine and carboxyl groups on the top hydrogel surface leads to low adhesion. Therefore, the coacervate-derived hydrogel exhibits asymmetric adhesiveness on the bottom and top surfaces. Moreover, the PEI/TA/TiO_2 hydrogel formed on the skin could be easily removed using a $NaHCO_3$ aqueous solution without inflicting damage. More importantly, the PEI/TA/TiO_2 hydrogel can function as an effective sunscreen to block UV light and prevent UV-induced MMP-9 overexpression, inflammation, and DNA damage in animal skin. The advantages of PEI/TA/TiO_2 coacervate-derived hydrogels include robust, asymmetric, and reversible wet bioadhesion, effective UV light-shielding ability, excellent biocompatibility, and easy preparation and usage, making them a promising bioadhesive to protect the skin from UV light-associated damage in wet and underwater environments.

1. Introduction

Ultraviolet light exposure is ubiquitous in our daily activities; however, long-term exposure to UV light causes severe skin morbidities, including skin sunburn, skin aging, and even skin cancers [1–3]. Depositing sunscreen on the skin is an effective approach to prevent them from UV light-induced skin morbidities [4,5]. Current commercial sunscreen agents can be divided into chemical sunscreen and physical sunscreen according to their ingredients. Chemical sunscreen contains organic filters, such as avobenzone, octinoxate, and avobenzone, which shield UV light by absorbing specific wavelengths of UV light [6–8]. However, organic filters can undergo photodegradation to generate

Peer review under responsibility of KeAi Communications Co., Ltd.
* Corresponding author.
** Corresponding author.
*** Corresponding author.
**** Corresponding author.
E-mail addresses: kyuzhang@scut.edu.cn (K. Zhang), xin.zhao@polyu.edu.hk (X. Zhao), gangli@cuhk.edu.hk (G. Li), bianlm@scut.edu.cn (L. Bian).
[1] These authors contributed equally to this work.

https://doi.org/10.1016/j.bioactmat.2023.07.016
Received 19 May 2023; Received in revised form 14 June 2023; Accepted 19 July 2023

carcinogenic free radicals and photoallergic/photosensitive reactions on the skin [9–11]. Compared with chemical sunscreen, physical sunscreen containing inorganic particulate filters (such as titanium dioxide (TiO_2) and zinc oxide (ZnO) particles) that can scatter and reflect UV light are more popular owing to their stability, non-toxicity, and low cost [8,12,13]. However, it is hard for the current commercial sunscreens to maintain effective and long-lasting UV light shielding in wet and underwater environments owing to their very weak adhesion to the skin.

Bioadhesive hydrogels that can tightly adhere onto tissues are promising biomaterials for diverse applications [14–18]. By introducing organic or inorganic filters into adhesive hydrogels, bioadhesive hydrogels can adhere onto the skin to protect it from UV light irradiation [19–24]. For example, by mixing polymers (such as thiolated hyaluronic acid) and polydopamine (PDA) nanoparticles that can absorb UV light and scavenge reactive oxygen species, Cheng and co-workers prepared a bioadhesive, water-resistant, and non-skin penetration hydrogel sunscreen, which demonstrates high UV light shielding efficiencies [20]. Xu and co-workers prepared a self-recovery and adhesive dual-network hydrogel sunscreen (DNHS) by using poly-γ-glutamic acid (γ-PGA) and tannic acid (TA), and this hydrogel can protect skin from UV light-induced skin morbidities [19]. However, it is challenging for these bulk hydrogels to effectively fill and fit into the irregular target sites and maintain long-lasting adhesion upon contacting sweat and water, thereby compromising the UV light protection efficiencies in wet and underwater environments. Moreover, these traditional adhesives are double-sided, with irreversible bioadhesion, which seriously limits their application.

To prepare adhesives with asymmetric adhesion, the Janus hydrogels and multilayer adhesives have been prepared [17,25,26]. Liu et al. reported a Janus hydrogel by immersing one side of a poly(*N*-acryloyl 2-glycine) (PACG) hydrogel into a chitooligosaccharide solution; the obtained hydrogel exhibited instant one-sided adhesion to tissues while preventing postoperative adhesion on the other side. Zhao et al. prepared an asymmetric adhesive consisting of a blood-repellent hydrophobic fluid layer, a microtextured bioadhesive layer, and an antifouling zwitterionic nonadhesive layer to mediate asymmetric adhesion. Nevertheless, most of these adhesive hydrogels demonstrate irreversible adhesion on the targeted substrates and are difficult to be removed from the substrates on demand, which may lead to harmful side effects. Increasing the cohesion of the adhesive hydrogel and weakening the interfacial adhesion between the adhesive hydrogel and the substrate can promote the detachment of the hydrogel from the substrate [27–29]. However, to the best of our knowledge, there is no prior work has demonstrated a hydrogel with robust, asymmetric, and on-demand reversible adhesion using a simple method.

Herein we prepared a PEI/TA/TiO_2 coacervate-derived hydrogel with robust, asymmetric, and on-demand reversible wet bioadhesion *via* a one-step process. By simply mixing the PEI aqueous solution and TA/TiO_2 powder, the PEI/TA/TiO_2 coacervate can be obtained. Upon depositing the PEI/TA/TiO_2 coacervate onto the skin, it can spread into surface irregularities, resulting in tight contact and interfacial adhesion between the coacervate bottom surface and the substrate. Subsequently, the solidification of the coacervate into the hydrogel with increased cohesion established an interdigitated contact, leading to robust adhesion to the substrate. The functional groups between the substrate and hydrogel can form physical interactions to further enhance bioadhesion. On the other hand, the non-fluidity and limited movement of the amine and carboxyl groups on the top hydrogel surface can reduce its adhesion to other substrates. Therefore, the coacervate-derived hydrogel can mediate asymmetric adhesion. Moreover, the PEI/TA/TiO_2 hydrogel deposited on the skin can be easily removed with a $NaHCO_3$ aqueous solution without damaging the underlying skin because HCO_3^- can decrease hydrogel cohesion and disrupt the physical interactions between the hydrogel and substrate. In addition, the incorporated TiO_2 nanoparticles can provide hydrogels with UV light-shielding ability. Moreover, we demonstrated that the PEI/TA/TiO_2 hydrogel can function as an effective sunscreen to better protect the skin from UV light-induced skin morbidities in nude mouse models compared with a commercial sunscreen.

2. Materials and methods

2.1. PEI/TA/TiO_2 coacervate and coacervate-derived hydrogel preparation

2.5 wt%, 5.0 wt%, 7.5 wt%, and 10 wt% TiO_2 nanoparticles (30 nm) were directly mixed 220 mg of TA powder, respectively. These powders were mixed with 1 mL of PEI aqueous solution (M_w = 1800, 10 wt%) through vortexing. Then the mixture was centrifuged to prepare PEI/TA/TiO_2 coacervate. Depositing PEI/TA/TiO_2 coacervate onto various substrates or injecting coacervate into custom mold, the hydrogel can spontaneously transfer to a hydrogel *in situ* without external stimuli.

2.2. Mechanical tests

All mechanical tests were performed with a Kinexus rheometer.

Rheological data of the hydrogels was measured using an 8-mm diameter flat plate. Gelation time of coacervate and storage modulus (G') of obtained hydrogel were conducted under a fixed strain of 1.0% and a frequency of 1 Hz at 37 °C. Lap shear tests were also performed with custom clamps at a crosshead speed of 3 mm min^{-1}. For lap shear tests, PEI/TA/TiO_2 coacervate and *ANESSA* were sandwiched between two pieces of porcine skin with an adhesion area of 2 cm × 1 cm, respectively. The adhesion stress was calculated as follows: Adhesion stress = $F_{max}/(wl)$, where F_{max} was the maximum force, and w and l were the width and length of the adhesion area. Compression tests were performed on cylindrically samples (thickness = 3 mm and diameter = 20 mm) at a crosshead speed of 1 mm min^{-1}. The compressive stress (σ_c) was calculated by σ_c = load/(πr^2) (r, the original radius of the specimen). The strain (ε_c) under compression was defined as the change in the thickness relative to the original thickness. Stress-strain data between ε_c = 1%–5% were used to calculate initial Young's modulus (E). Three specimens were tested to ensure the reliability of the data.

2.3. In vitro biocompatibility test

Biocompatibility of PEI/TA/TiO_2 hydrogel was tested by using a direct contact method between 3T3 cells and hydrogel. Dulbecco's modified eagle medium (DMEM) was used as the complete growth medium. 3T3 cells were added at a density of 25,000 cells/well and incubated in 5% CO_2 humidified atmosphere at 37 °C for 12 h. Then, 100 mg PEI/TA/TiO_2 hydrogel was put into the wells with cells. Growth medium without hydrogel was used as a positive control. After incubation for 24 h, cell viability was evaluated by the Live/Dead cell staining method.

2.4. Adhesion test

Depositing fluorescent PEI/TA/TiO_2 coacervate and commercial sunscreen *ANESSA* onto a piece of porcine skin and immersing samples in artificial sweat. 12 h later, the samples were frozen in optimal cutting temperature compound (OCT) and cut into 25-μm sections, which were observed through confocal microscope.

2.5. Reversible adhesion

Immersing PEI/TA/TiO_2 hydrogel into $NaHCO_3$ (1 mol L^{-1}) aqueous solution, and then measuring their *stiffness* through compression test. Wetting gauze with $NaHCO_3$ solution, then covering the gauze onto the PEI/TA/TiO_2 hydrogel adhered to tissue, resulting in easy removal of the adhered hydrogel.

2.6. UV light shielding ratio measurement

PEI/TA/TiO_2 coacervate-derived hydrogel and commercial sunscreen *ANESSA* were deposited on clean quartz plate, and these quartz plates were immersed in artificial sweat (pH = 6.6). At pre-set time point, these quartz plates were irradiated under a 311 nm UV-LED light, and the light power was measured by using a 311 nm light power meter. The UV light shielding ratio was calculated as follows: $(J_0 - J)/J \times 100\%$, where J_0 and J were light power under clean quartz plate and quartz plate painted with different samples.

2.7. In vitro UV light protection evaluation

3T3 cells (8×10^4/well) that cultured in 12-well plate were divided into four groups (normal group, PEI/TA/TiO_2 hydrogel group, *ANESSA* group and non-protection group), and the quartz plates painted with different sunscreen were immersed in artificial sweat for 1 h before they were fixed at 1 cm above the cell culture wells. Then the UV light irradiation groups were irradiated 180 mJ cm^{-2} of UVB (311 nm). Cell viability was measured by using the alarm blue assay and observed by a calcein-AM/propidium iodide live-dead staining. Moreover, the ROS generation in 3T3 cells were tested by using an oxidation-sensitive fluorescent probe (5-(and-6)-carboxy-20, 70-dichlorodihydrofluorescein diacetate, abbreviated as carboxy-H2DCFDA).

2.8. In vivo UV light protection evaluation

Female nude mice with an average weight of 20 g were used in this study. The tissue damage induced by UVA is known to take a long time. Therefore, in order to evaluate the efficacy of hydrogel to reduce UV-induced skin damage in a short experimental period, we choose UVB as the UV irradiation, which can cause skin damage rapidly, according to previous work about the sunscreen [19,20,30]. Depositing *ANESSA* or PEI/TA/TiO_2 hydrogel onto dorsal skin of nude mice and flushing them with artificial sweat for 10 min. One hour later, these mice were exposed under UV light (311 nm, 240 mJ cm^{-2}) each day for 5 days, and mice without any protection and normal mice were used as positive and negative control, respectively. The mice were euthanized two days after the final irradiation to allow the recovery from the acute UVB irradiation. Six rats for each group. And the dorsal skin was fixed in phosphate-buffered formalin for 24h, dehydrated, and embedded in paraffin. Paraffin-embedded samples were cut into 7-μm sections, which were deparaffinized by using xylene and dehydrated using gradient alcohol. Then, the sections were stained with hematoxylin-eosin (H&E) and Masson's trichome. The study was approved by the Animal Experimentation Ethics Committee of the Chinese University of Hong Kong (21-034-MIS).

2.9. Immunofluorescence (IF) staining

Samples were firstly dewaxed using xylene, dehydrated by using gradient alcohol, and washed in PBS twice. After incubating samples in 1% normal serum block, the samples were incubated in primary antibody, matrix metalloproteinase-9 (MMP-9), interleukin 6 (IL-6) and γH2AX at 4 °C overnight in dark. After being washing with PBS for three times, the secondary antibody was used to incubate the samples at room temperature for 2 h in dark. Then, the samples were washed with PBS three times before being incubated with fluorescent avidin at room temperature for 30 min in dark. Finally, after washing with PBS for twice, the samples were counterstain with DAPI for 20 min at room temperature.

2.10. Statistical analysis

All data were shown as means ± SD via at least triplicate samples. Independent Student's *t*-test and one-way ANOVA followed by a Tukey *post hoc* analysis were used to determine statistical significance between two or multiple groups, respectively. Statistical analyses were performed using SPSS (Statistical Package for the Social Sciences) 25.0, and a two-sided $P < 0.05$ was considered statistically significant.

3. Results and discussion

3.1. Preparation and properties of PEI/TA/TiO_2 coacervate-derived hydrogel

The preparation of the PEI/TA/TiO_2 coacervate and coacervate-derived hydrogels is shown in Fig. 1a. By mixing 1 mL of PEI aqueous solution (M_w = 1800, 10 wt%) with TA powder (220 mg) and TiO_2 nanoparticles (30 nm), TA interacted with PEI through electrostatic interactions and hydrogen bonding. TiO_2 interacted with TA or PEI through hydrogen bonding, and the hydrophobic disulfide ring and alkyl chain in TA aggregated to form a hydrophobic cross-linking domain, resulting in the formation of a PEI/TA/TiO_2 complex suspension (Fig. 1a2). Then, by gently centrifuging the PEI/TA/TiO_2 complex suspension, the complex aggregated to induce macroscopic fluid−fluid phase separation, generating a dense PEI/TA/TiO_2 coacervate phase and a dilute phase (Fig. 1a3). Finally, the PEI/TA/TiO_2 coacervate phase was further stabilized, possibly because of the continued aggregation of hydrophobic 1,2-dithiolanes in TA molecules and physical interactions among PEI, TA, and TiO_2 [31], leading to the spontaneous transition from the PEI/TA/TiO_2 coacervate to the PEI/TA/TiO_2 hydrogel (Fig. 1a4). Moreover, upon injecting the PEI/TA/TiO_2 coacervate into a pentagram mold, it can spontaneously transfer to a pentagram hydrogel without external stimuli, indicating that this coacervate can form hydrogel of custom shape according to the shape of the target site (Fig. 1b). To use this coacervate-derived hydrogel more conveniently in daily life, the PEI aqueous solution and TA/TiO_2 powder were stored in two independent plastic bags. The PEI solution was squeezed into the TA/TiO_2 powder and mixed fully in a bag, the PEI/TA/TiO_2 coacervate can also be obtained. By depositing the coacervate onto a glass plate, it can be transformed into a hydrogel *in situ*, which can strongly adhere to the glass despite being flushed with water (Fig. S1). In addition, after co-incubating the 3T3 cells with the PEI/TA/TiO_2 hydrogel, the cells demonstrated excellent cell viability, with no significant difference from that of the positive control group (Fig. 1c). This result indicated the excellent cytobiocompatibility of the PEI/TA/TiO_2 hydrogel, which is important for biomedical materials used on the skin.

The crosslinking mechanism of the PEI/TA/TiO_2 gel was studied using Fourier Transform Infrared (FTIR) spectrum characterization. The infrared characteristic peaks of the amine groups in PEI (1572 cm^{-1}), carboxylic acid group in TA (1691 cm^{-1}), and Ti–O bond in TiO_2 (638 cm^{-1}) shifted to 1536 cm^{-1}, 1642 cm^{-1}, and 611 cm^{-1}, respectively, instead of forming new characteristic peaks (Fig. 1d). This indicates that PEI, TA, and TiO_2 in the PEI/TA/TiO_2 hydrogel were crosslinked through physical interactions, such as hydrogen bonding and electrostatic interactions.

In addition, the gelation time of the PEI/TA/TiO_2 coacervate and mechanical properties of the coacervate-derived hydrogel were adjusted by changing the content of TiO_2. Increasing the content of TiO_2 nanoparticles from 0 to 10 wt%, the gelation time of PEI/TA/TiO_2 coacervate decreased from 174 ± 9 to 33 ± 8 s (Fig. 1e). Meanwhile, the storage modulus (G') of the coacervate-derived hydrogel increased with increasing TiO_2 nanoparticle content because more TiO_2 nanoparticles could form denser cross-linking densities in the hydrogel (Fig. 1f). Moreover, the adhesion stress increased with increasing TiO_2 nanoparticle content owing to stronger cohesion (Fig. S2). Therefore, the addition of TiO_2 nanoparticles to the coacervate significantly improved the mechanical and adhesive properties of the PEI/TA/TiO_2 coacervate-derived hydrogel. To balance the gelation time of the PEI/TA/TiO_2 coacervate and mechanical properties of the coacervate-derived hydrogel, we used an intermediate 5 wt% TiO_2 nanoparticles content

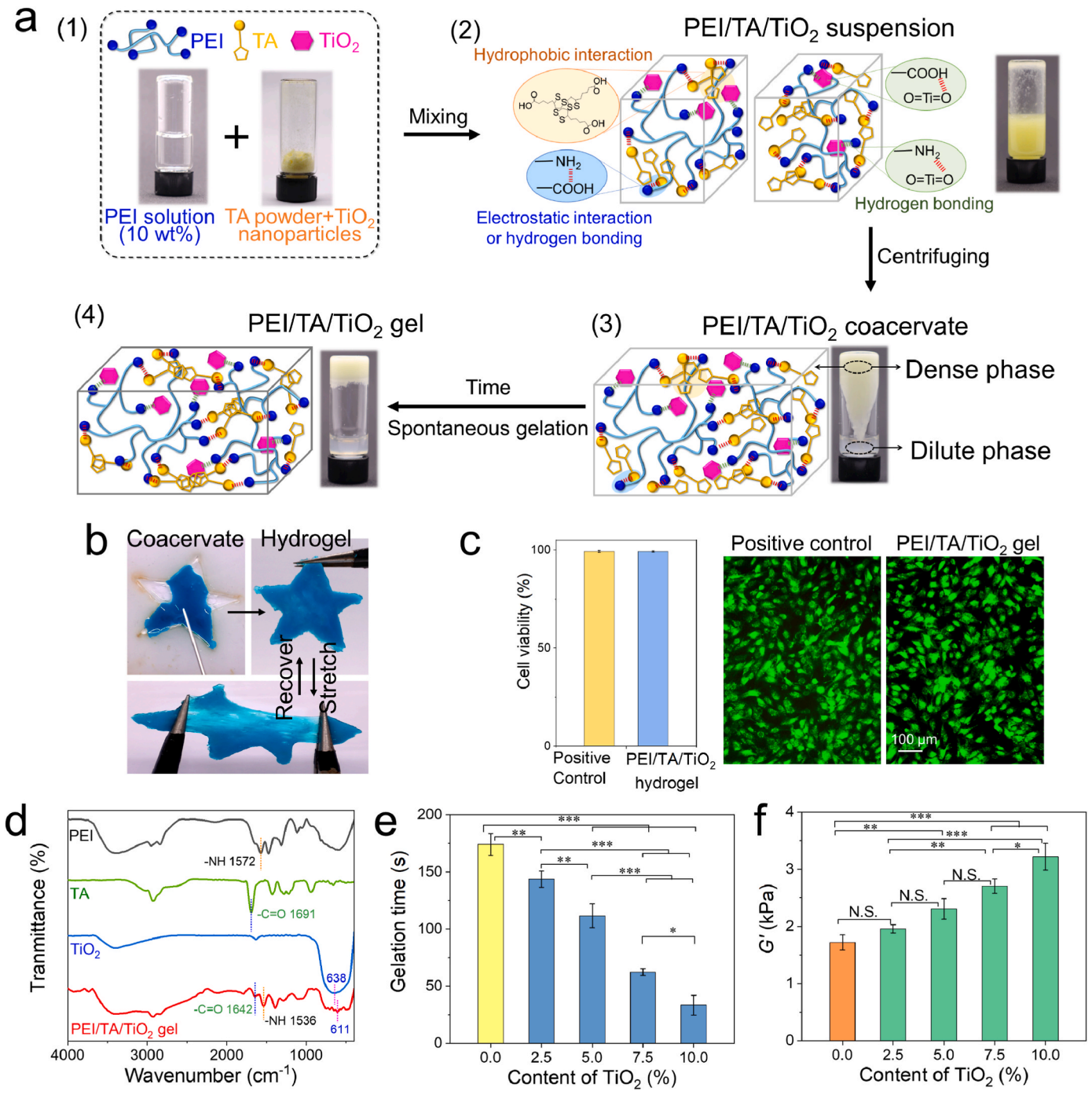

Fig. 1. Preparation and properties of PEI/TA/TiO_2 coacervate and coacervate-derived hydrogel. (a) Schematic illustration and process of the formation of PEI/TA/TiO_2 coacervate and coacervate-derived hydrogel. (b) Injection of PEI/TA/TiO_2 coacervate into a pentagram model for fabricating the pentagram-shaped hydrogel. (c) Cell viability (left) and live/dead staining (right) of 3T3 cells after being co-incubated with PEI/TA/TiO_2 hydrogel or positive control media for 24 h ($n = 3$). (d) FTIR spectra of the PEI, TA, TiO_2, and PEI/TA/TiO_2 coacervate-derived gel. (e) Gelation time of PEI/TA/TiO_2 coacervate prepared with varying content of TiO_2 nanoparticles. Test Conditions: 37 °C in PBS ($n = 3$). (f) Storage modulus (G') of cylindrical PEI/TA/TiO_2 coacervate-derived hydrogels with varying content of TiO_2 nanoparticles after gelation at 37 °C for 3 min ($n = 3$). Statistical significance was analyzed by one-way ANOVA followed by a Tukey *post hoc* analysis between multi-groups, $^{N.S.}P > 0.5$, $^{*}P < 0.05$, $^{**}P < 0.01$ and $^{***}P < 0.001$.

in subsequent experiments.

3.2. Asymmetric bioadhesion of PEI/TA/TiO_2 coacervate-derived hydrogel

First, we studied the robust adhesion of the PEI/TA/TiO_2 coacervate-derived hydrogel. Owing to the fluidity of the PEI/TA/TiO_2 coacervate, it can spread into the surface irregularities of the substrate to form tight contact between its bottom surface and the substrate. The subsequent spontaneous solidification of the coacervate into the hydrogel resulted in increased cohesion and interdigitated contact with the substrate, leading to robust adhesion between the bottom surface of the hydrogel and substrate. The functional groups on the substrate surface and bottom surfaces of the hydrogel can form physical interactions (such as hydrogen bonding and electrostatic interactions) to enhance adhesion (Fig. 2a). Therefore, after depositing the PEI/TA/TiO_2 coacervate

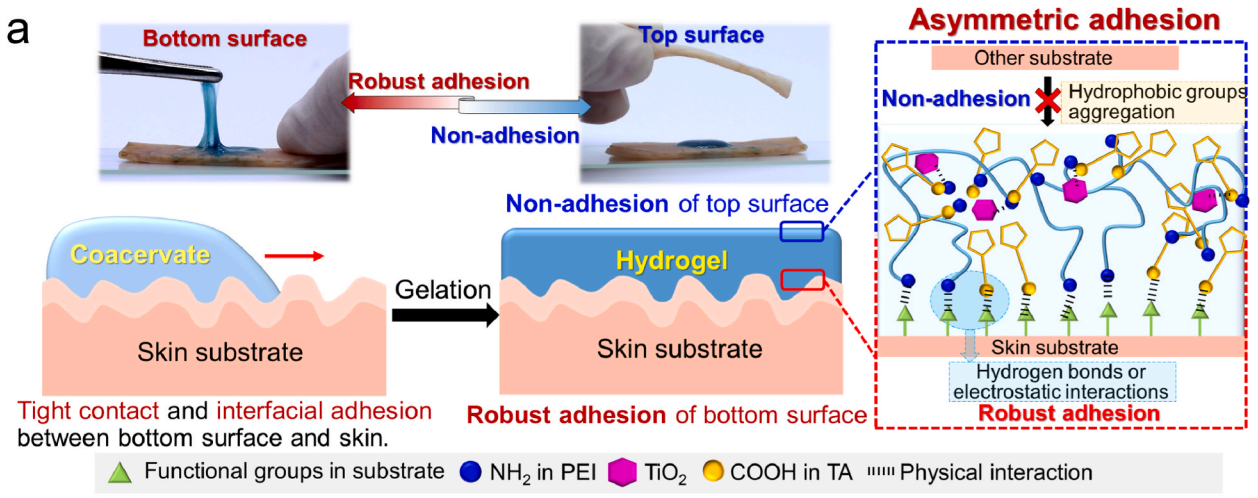

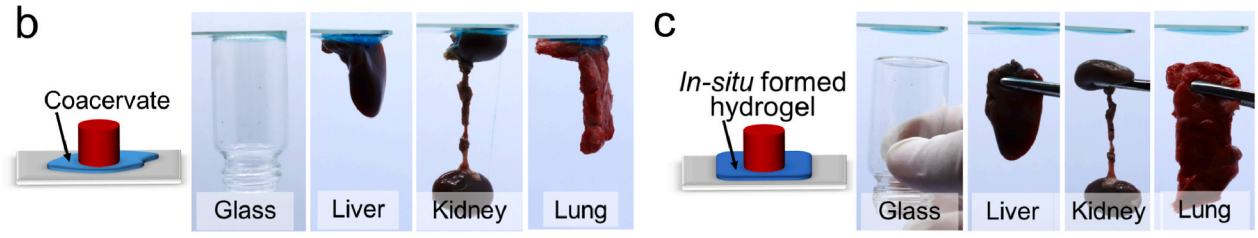

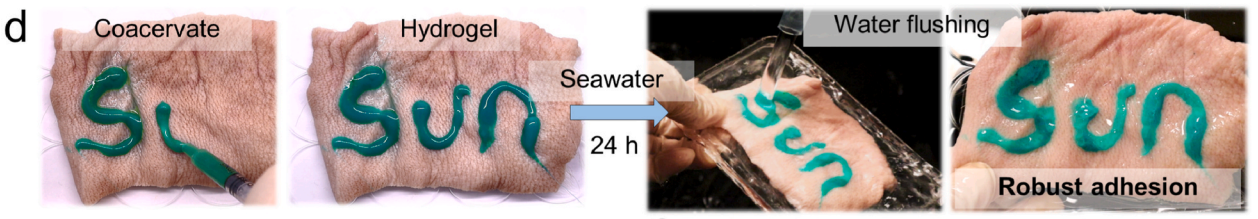

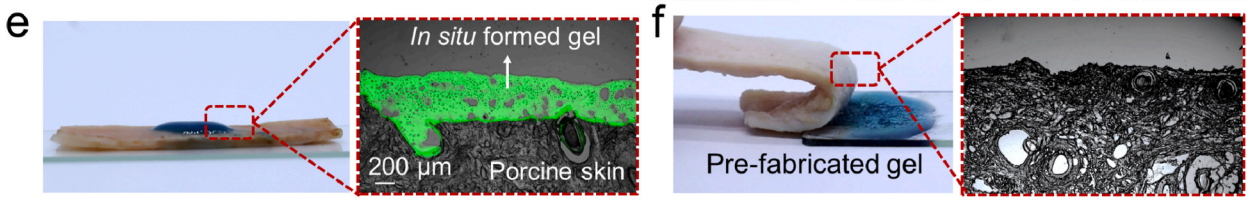

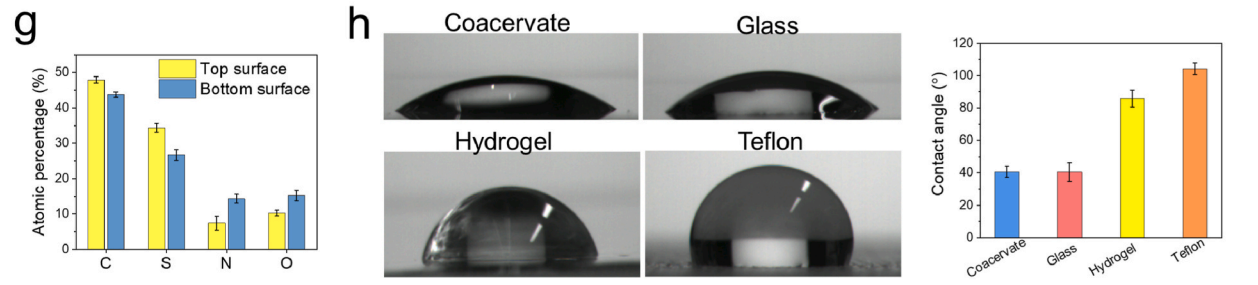

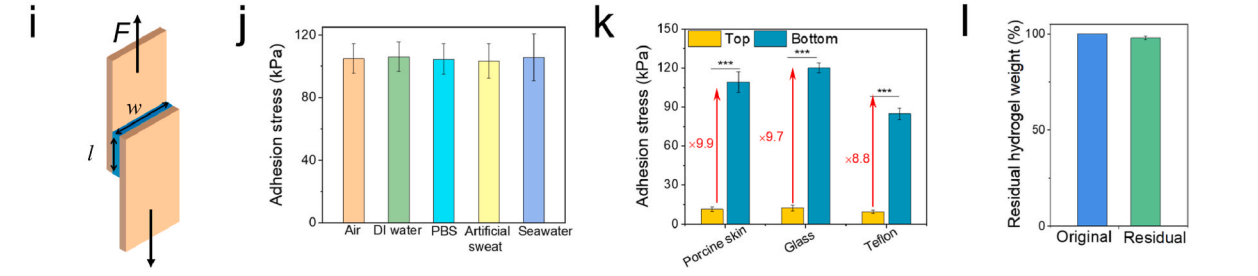

(caption on next page)

Fig. 2. Asymmetric bioadhesion of PEI/TA/TiO_2 coacervate-derived hydrogel. (a) Schematic illustration of the asymmetric bioadhesion of PEI/TA/TiO_2 coacervate-derived hydrogel. (b, c) Robust adhesion of the bottom surface (b) and non-adhesion of the top surface (b) of the PEI/TA/TiO_2 coacervate-derived hydrogel. (d) Robust adhesion of PEI/TA/TiO_2 coacervate-derived hydrogel on a piece of porcine skin. (e) Tight contact between the bottom surface and *in situ* formed hydrogel. (f) Non-contact between the top surface and pre-fabricated hydrogel. (g) Atomic percentage of the top and bottom surfaces of the hydrogel. (h) Contact angles of water on various substrates including coacervate, glass plate, *in situ* formed hydrogel, and Teflon ($n = 6$). (i) Schematic illustration for lap shear test. (j) Adhesion stress of PEI/TA/TiO_2 coacervate-derived hydrogel before and after being immersed in various solutions including de-ionized water, PBS, artificial sweat, and seawater. (k) Asymmetric adhesion stress of the top and bottom surfaces of the hydrogel. (l) Weight of the hydrogel before and after being pressed onto a piece of the porcine skin. Statistical significance was calculated by Student's *t*-test. ***$P < 0.001$. Data are shown as the mean ± SD.

between a piece of glass plate and glass bottle or tissues (such as the liver, kidney, or lung), these objects can tightly adhere together (Fig. 2b). Moreover, the PEI/TA/TiO_2 coacervate injected onto a piece of porcine skin transformed into a hydrogel *in situ* and tightly adhered to the porcine skin without any detachment, even after immersion in seawater for 24 h and flushing with water (Fig. 2d). The adhesion of the PEI/TA/TiO_2 hydrogel was quantitatively evaluated using a lap shear test (Fig. 2i). After adhering two pieces of porcine skins with PEI/TA/TiO_2 coacervate-derived hydrogel and then immersing them into various aqueous solutions at 37 °C for 24 h, the adhesion stress between the porcine skins remained stable, indicating the robust and stable wet adhesion of the PEI/TA/TiO_2 coacervate-derived hydrogel (Fig. 2j).

Next, the asymmetric adhesion of the PEI/TA/TiO_2 coacervate-derived hydrogels was studied. Pressing a glass bottle or some tissues (such as the liver, kidney, and lung) onto a prefabricated PEI/TA/TiO_2 hydrogel, the hydrogel could not adhere to these objects, indicating nonadhesion of the top surface of the hydrogel (Fig. 2c). To study the non-adhesive mechanism of the top surface, we first studied the interface between the hydrogel and porcine skin (Fig. 2e and f). By depositing the PEI/TA/TiO_2 coacervate onto a piece of porcine skin, the coacervate can spread into the surface irregularities of the substrate to form a tight contact between its bottom surface and the substrate. In contrast, by pressing a piece of porcine skin onto a prefabricated PEI/TA/TiO_2 hydrogel, the hydrogel could not spread into the surface irregularities of the substrate, resulting in weak contact between the top surface of the hydrogel and substrate (Fig. 2f). These results demonstrate that the non-fluidity of the prefabricated PEI/TA/TiO_2 hydrogel limits the close contact between the top surface and substrate. We further tested the elemental compositions of the top and bottom surfaces using a scanning electron microscope equipped with an energy-dispersive X-ray spectroscope (SEM-EDX). The atomic percentages of C and S (47.9 ± 0.9% and 34.4 ± 1.2%) in the top hydrogel surface were significantly higher than those in the bottom surface (43.7 ± 0.7% and 26.7 ± 1.5%), and the atomic percentage of N and O in top hydrogel surface (7.4 ± 2.0% and 10.3 ± 0.8%) were lower than those in the bottom surface (14.3 ± 1.2% and 15.3 ± 1.5%), indicating that the 1,2-dithiolanes groups instead of the adhesive groups (such as amine and carboxyl groups) predominantly aggregated in the top hydrogel surface network (Fig. 2g). The water contact angle on PEI/TA/TiO_2 coacervate-derived hydrogel (85.8 ± 5.1°) was similar to that on the hydrophobic Teflon (104.2 ± 3.5°) and was much higher than that on coacervate (40.7 ± 3.5°) and glass plate (40.4 ± 5.7°), further indicating that the hydrophobic 1,2-dithiolanes groups aggregated in the top hydrogel surface network (Fig. 2h). These results indicate that the crosslinked network of the coacervate-derived hydrogel limited the free movement of the amine and carboxyl groups on the top surface. In addition, we quantitatively evaluated the asymmetric adhesion of the top and bottom surfaces of the PEI/TA/TiO_2 coacervate-derived hydrogels. The adhesion stress of the bottom hydrogel surface on porcine skin, glass, and Teflon (108 ± 8.1, 120 ± 3.8, 84.7 ± 4.5 kPa) was much higher than those of the top hydrogel surface (11.4 ± 1.7, 12.3 ± 2.1, 9.5 ± 1.2 kPa) (Fig. 2k). Moreover, after pressing a piece of porcine skin onto the prefabricated PEI/TA/TiO_2 hydrogel and removing it, approximately no decrease in the weight of the hydrogel was observed, indicating a low adhesive property of the top hydrogel surface (Fig. 2l).

3.3. On-demand removability of adherent PEI/TA/TiO_2 coacervate-derived hydrogel

Because the adhesion between the PEI/TA/TiO_2 coacervate-derived hydrogel and substrate was based on interdigitated contact and physical interactions, we decreased the cohesion of the hydrogel and weakened the physical interactions between the hydrogel and tissue to remove the adherent hydrogel (Fig. 3a). By immersing PEI/TA/TiO_2 hydrogel in $NaHCO_3$ aqueous solution at 37 °C, the hydrogel Young's moduli (E) decreased over time, indicating the decreasing cross-linking densities and cohesion of the hydrogel (Fig. S3). Therefore, by applying a gauze wetted with $NaHCO_3$ aqueous solution, the PEI/TA/TiO_2 hydrogel deposited on the porcine skin can be easily removed without residual gel because HCO_3^- can decrease hydrogel cohesion and disrupt physical interactions between the hydrogel and substrate (Fig. 3b). The adhesion stress of the hydrogel significantly decreased over time after immersing the samples in a $NaHCO_3$ aqueous solution at 37 °C (Fig. 3c). Next, we deposited the PEI/TA/TiO_2 coacervate onto the backs of nude mice and removed the PEI/TA/TiO_2 coacervate-derived hydrogel with wet gauze containing $NaHCO_3$ aqueous solution. Hematoxylin and eosin (H&E) staining revealed no notable difference in the skin structure between the experimental and control groups, indicating minimal skin damage due to the removal of the PEI/TA/TiO_2 hydrogel (Fig. 3d). Therefore, the tissue-adherent PEI/TA/TiO_2 coacervate-derived hydrogel could be removed on demand with minimal damage to the substrate tissue.

3.4. Effective protection against UV light irradiation by PEI/TA/TiO_2 hydrogel

Adding TiO_2 nanoparticles to the coacervate not only significantly improved the mechanical and adhesive properties of the PEI/TA/TiO_2 coacervate-derived hydrogel but also endowed the hydrogel with the capability to shield covered tissues from UV light exposure. We first compared the UV light-shielding ratio of the PEI/TA/TiO_2 hydrogel and commercial sunscreen *ANESSA* containing TiO_2 and ZnO. After depositing the two samples onto a quartz plate, the UV light shielding ratio was determined by testing the power of the UV light under a clean quartz plate and quartz plate painted with different samples (Fig. 4a). Under dry conditions, the UV-light-shielding ratios of the PEI/TA/TiO_2 hydrogel and *ANESSA* were approximately 100%. After immersion in artificial sweat (pH = 6.6) for 12 h, the UV shielding ratio of the PEI/TA/TiO_2 hydrogel remained above 96% owing to the strong underwater adhesion of the PEI/TA/TiO_2 hydrogel, whereas the UV shielding ratio of *ANESSA* dramatically decreased from 100% to 6.7% owing to the detachment of *ANESSA* from the artificial sweat (Fig. 4b and Fig. S4).

Next, we compared *in vitro* UV light protection mediated by the PEI/TA/TiO_2 hydrogel and *ANESSA* upon contact with artificial sweat by depositing different samples onto quartz plates, immersing them in artificial sweat for 1 h, and then placing them between the UV source and 3T3 cells (Fig. 4c). After exposure to UV light (311 nm, 240 mJ cm^{-2}) for 15 min, cells in the unprotected group showed notable apoptosis. The cells in the PEI/TA/TiO_2 hydrogel group remained viable, with no significant difference from the normal cells, whereas the *ANESSA* group demonstrated relatively lower cell survival. Moreover, the results of the Alamar blue assay revealed that the PEI/TA/TiO_2 hydrogel group demonstrated cell viability similar to that of the normal

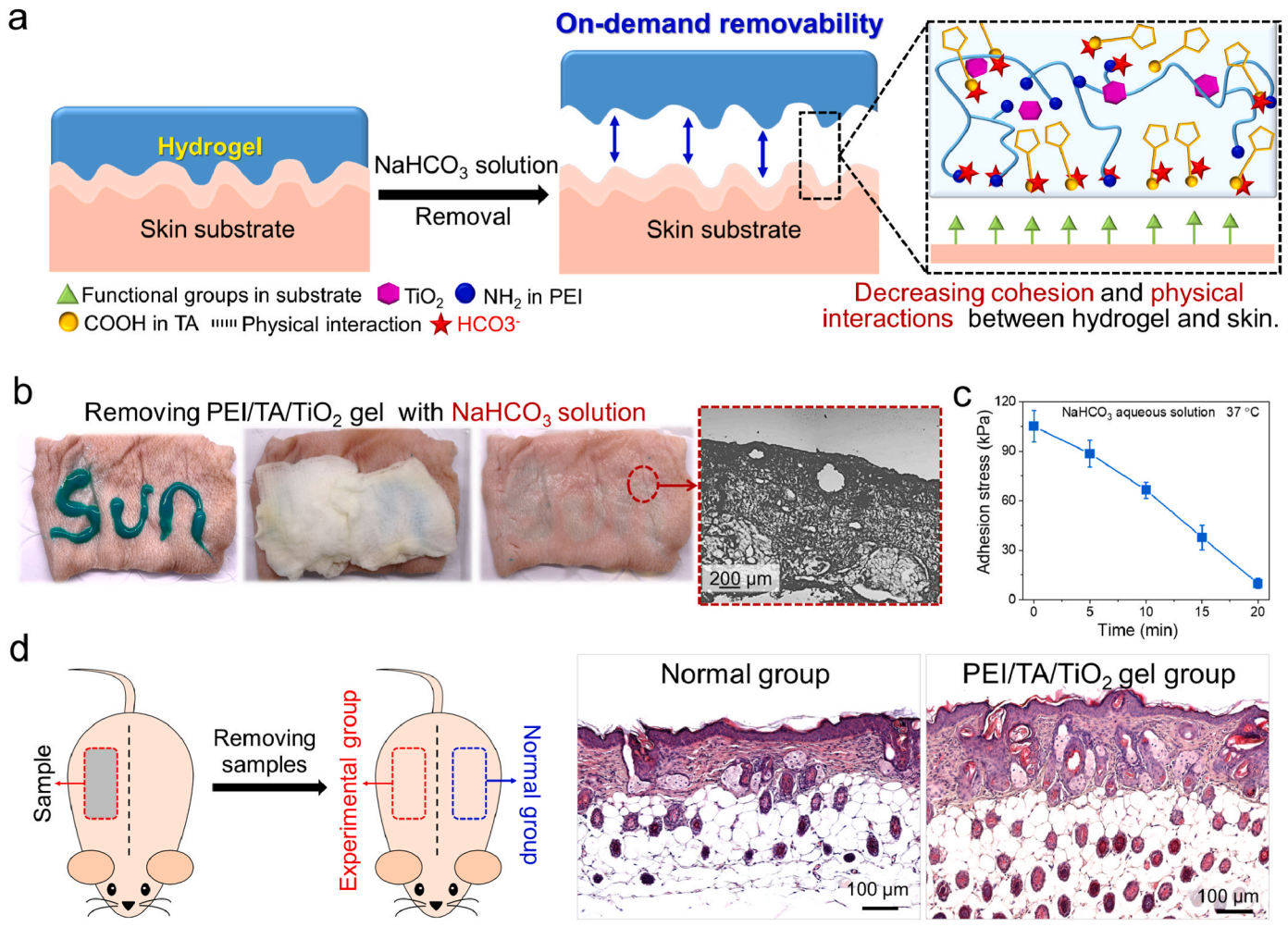

Fig. 3. On-demand removability of PEI/TA/TiO_2 coacervate-derived hydrogel. (a) Schematic illustration of the removal of PEI/TA/TiO_2 hydrogel deposited on a substrate. (b) Removal of PEI/TA/TiO_2 hydrogel deposited on the porcine skin with a gauze wetted with a $NaHCO_3$ aqueous solution. (c) Adhesion stress of PEI/TA/TiO_2 hydrogel after being immersed in a $NaHCO_3$ aqueous solution at 37 °C for different times ($n = 3$). (d) H&E staining of the normal skin (left) and skin after removing a PEI/TA/TiO_2 coacervate-derived hydrogel with a wet gauze containing a $NaHCO_3$ aqueous solution (right). Data are shown as the mean ± SD.

group ($P = 0.46$), which was much higher than that of the *ANESSA* and non-protected groups ($P < 0.001$ and $P < 0.001$, respectively) (Fig. 4d). These results indicate the effective and long-lasting UV light-shielding ability of the PEI/TA/TiO_2 hydrogel in wet or underwater environments.

3.5. PEI/TA/TiO_2 hydrogel-mediated effective shielding against UV light irradiation in an animal model

Next, we compared the capabilities of the PEI/TA/TiO_2 hydrogel and *ANESSA* to protect against UV irradiation in a nude mouse skin model by first depositing the PEI/TA/TiO_2 hydrogel and *ANESSA* onto the dorsal skin of nude mice and flushing them with artificial sweat for 10 min (Fig. 5a). One hour later, the mice were exposed to UV light (240 mJ cm^{-2}) for 20 min per day. Mice without protection and normal mice were used as positive and negative controls, respectively. After five days of UV light irradiation, the dorsal skin of mice treated with the PEI/TA/TiO_2 hydrogel demonstrated no noticeable difference from that of the normal group, whereas the dorsal skin of non-protected mice demonstrated significant damage (Fig. 5b). The integrity of dorsal skin from different groups was further investigated using H&E staining. In the unprotected group, the dorsal skin demonstrated significant acanthosis and epidermal hyperplasia. In the PEI/TA/TiO_2 hydrogel group, the dorsal skin demonstrated no obvious differences compared to the normal skin. The epidermal thickness of the PEI/TA/TiO_2 hydrogel group was similar to that of the normal group ($P < 0.001$) and much thinner than that of the non-protection group ($P > 0.05$). In the *ANESSA* group, the dorsal skin showed slight epidermal hyperplasia ($P < 0.001$), indicating slight UV damage (Fig. 5c). Moreover, after trichrome staining, the PEI/TA/TiO_2 hydrogel-treated group showed no detectable keratin overproduction and a similar relative keratin percentage to that of the normal group ($P > 0.05$). By contrast, keratin overproduction was significant in the unprotected and *ANESSA* groups ($P < 0.001$ and $P < 0.001$, respectively), which could cause skin irritation or keratosis pilaris (Fig. 5d). These results indicated the effective protection of animal skin by the PEI/TA/TiO_2 hydrogel against UV light irradiation.

Next, we performed IF staining for MMP-9 (a member of the matrix metalloproteinase enzyme family capable of degrading extracellular matrix proteins to induce skin photoaging) and IL-6 (an interleukin that acts as a pro-inflammatory cytokine). As shown in Fig. 5e, no overexpression of MMP-9 was observed in the PEI/TA/TiO_2 gel group than in the normal group ($P > 0.05$). However, the non-protected group and *ANESSA* group demonstrated the overexpression of MMP-9 (red arrow) by 5.6- and 3.8-fold, respectively, compared to the normal group ($P < 0.001$ and $P < 0.001$, respectively). In addition, IL-6 staining (green arrow) showed that inflammation in the PEI/TA/TiO_2 gel group and normal group was not significantly different ($P > 0.05$), whereas skin inflammation in the non-protection group ($P < 0.001$) and *ANESSA* group ($P < 0.001$) was more severe than that in the normal group.

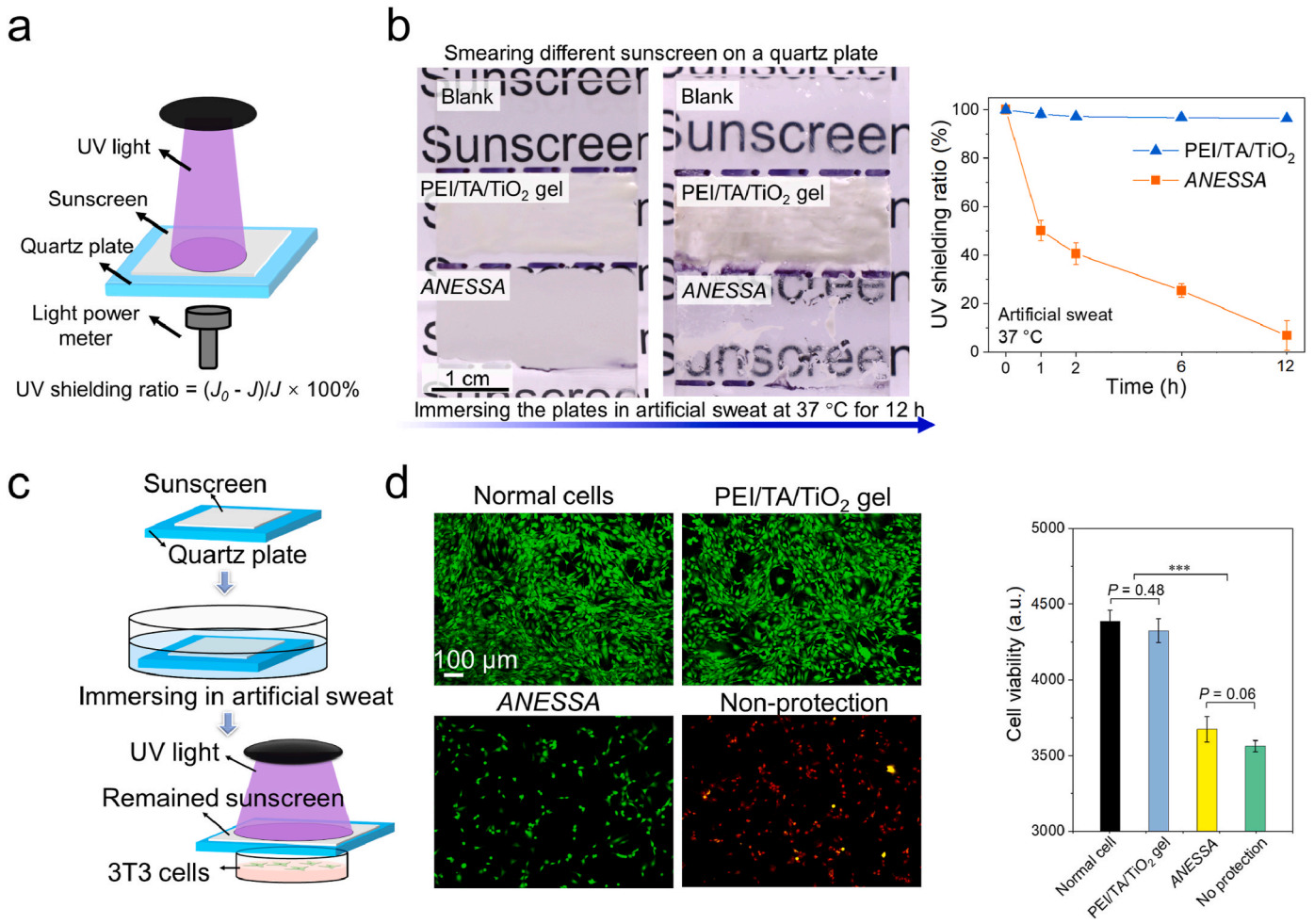

Fig. 4. *In vitro* protection against UV light irradiation mediated by PEI/TA/TiO_2 hydrogel. (a) Schematic illustration for measuring UV shielding ratio. J_0 and J represent the light powers under clean quartz plates and quartz plates painted with different samples, respectively. (b) Photos and UV light shielding ratio of different samples on a quartz plate before and after being immersed in artificial sweat at 37 °C. (c) Schematic illustration for assessment of *in vitro* UV light protection of different samples. (d) Live/Dead staining (left) and cell viability (right) of 3T3 cells in different groups containing normal cells, cells protected with PEI/TA/TiO_2 hydrogel and *ANESSA*, and cells with non-protection. Data are shown as the mean ± SD. Statistical significance was analyzed by one-way ANOVA followed by a Tukey *post hoc* analysis among four groups, ***$P < 0.001$.

In addition, UV irradiation-induced ROS *in vitro* and DNA damage in animal skin were evaluated. We first used an oxidation-sensitive fluorescent probe, carboxy-H2DCFDA, to labeled the UV exposure-induced ROS 3T3 cells [20]. Direct UV irradiation generated substantial ROS in 3T3 cells, whereas ROS generation was significantly reduced by covering the cells with the PEI/TA/TiO_2 hydrogel. The inhibition efficiency of UV light-induced ROS generation by the PEI/TA/TiO_2 hydrogel was much higher than that of *ANESSA* as determined by the ROS-positive cell ratio ($P < 0.001$) (Fig. 6a and S5). Moreover, the ROS can react with cellular DNA and lead to double-strand breaks (DSBs), which can be examined by the phosphorylated histone H2A variant H2AX (γH2AX) staining [20,30]. As shown in Fig. 6b, γH2AX staining showed that DSBs in the PEI/TA/TiO_2 gel group and normal group was not significantly different, whereas DSBs in the non-protection group and *ANESSA* group were more severe than that in the normal group.

These results indicated that the PEI/TA/TiO_2 hydrogel can function as an effective sunscreen to block UV light and prevent UV-induced MMP-9 overexpression, inflammation and DNA damage in animal skin.

4. Conclusion

In conclusion, the PEI/TA/TiO_2 coacervate-derived hydrogel demonstrates robust, asymmetric, and on-demand reversible wet bioadhesion and can also effectively protect the skin from UV light-induced damage in wet and underwater environments. The PEI/TA/TiO_2 coacervate was easily prepared by mixing a PEI aqueous solution with TA/TiO_2 powder and centrifuging the mixture. The PEI/TA/TiO_2 coacervate deposited on the skin can spread into surface irregularities, resulting in tight contact between them. Subsequently, the solidification of the coacervate to the hydrogel with increased cohesion establishes interdigitated contact and adhesion with the skin. The functional groups between the substrate and hydrogel can form physical interactions to further enhance adhesion. However, owing to the non-fluidity and limited movement of the amine and carboxyl groups in the top surface network of the hydrogel after the coacervate-to-hydrogel transition, the top hydrogel surface demonstrated poor adhesive properties. Moreover, the PEI/TA/TiO_2 hydrogel deposited on the skin can be removed with a $NaHCO_3$ aqueous solution because HCO_3^- can decrease hydrogel cohesion and disrupt the physical interactions between the hydrogel and substrate. Owing to the presence of TiO_2 nanoparticles, the PEI/TA/TiO_2 hydrogel can effectively absorb and reflect UV light, resulting in excellent UV light-shielding capability. Therefore, the PEI/TA/TiO_2 coacervate-derived hydrogel can effectively protect the skin from UV light-induced damage in wet and underwater environments. This study demonstrates a promising strategy for developing advanced UV-

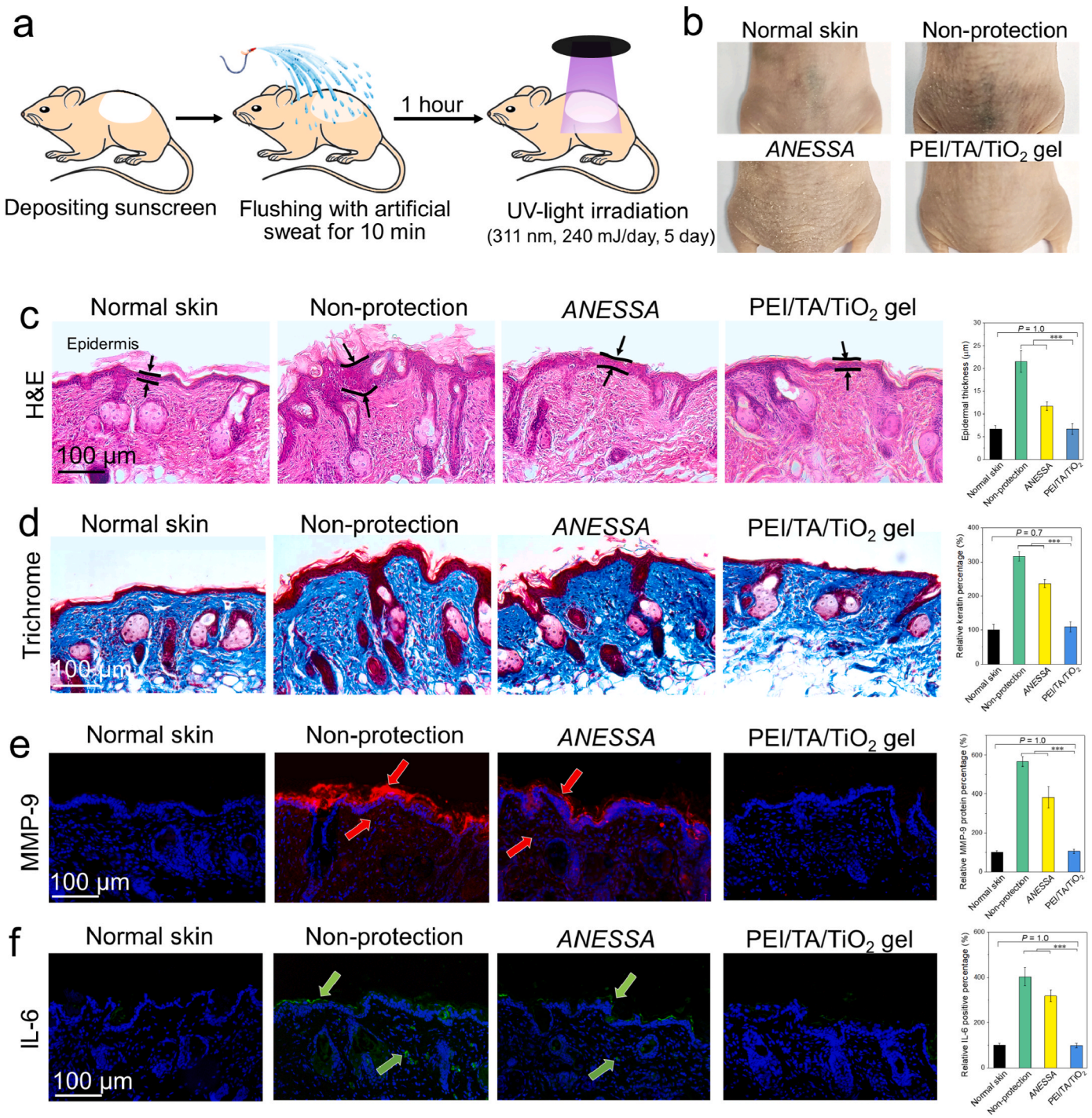

Fig. 5. Effective protection of animal skin against UV light irradiation by PEI/TA/TiO_2 hydrogel sunscreen. (a) Schematic illustration for assessment of the UV light-shielding efficacy of different samples. (b) Photos of the dorsal mouse skin of different groups including the normal group, non-protection group, *ANESSA* group, and PEI/TA/TiO_2 hydrogel group. (c) Hematoxylin/eosin staining (left) and epidermal thickness (right) of different groups. (d) Trichrome staining (left) and relative keratin percentage (right) of different groups. (e) MMP-9 staining (left, red arrow) and relative MMP-9 protein expression percentage (right) of different groups. (f) IL-6 staining (left, green arrow) and relative IL-6 positive expression percentage (right) of different groups. Mice, $n = 6$. Data are shown as the mean ± SD. Statistical significance was analyzed by one-way ANOVA followed by a Tukey *post hoc* analysis between three groups, $^{***}P < 0.001$.

shielding biomaterials based on a unique coacervate–hydrogel transition process.

Data availability statement

The data that support the findings of this study are available from the corresponding author upon reasonable request.

CRediT authorship contribution statement

Xin Peng: Investigation, Methodology, Validation, Data collection, Data curation, Original manuscript writing and revision. **Yuan Li:** Animal model construction, Tissue sections collection. **Menghui Liu:** Animal model construction, Tissue sections collection. **Zhuo Li:** Methodology, Manuscript writing suggestions. **Xuemei Wang:**

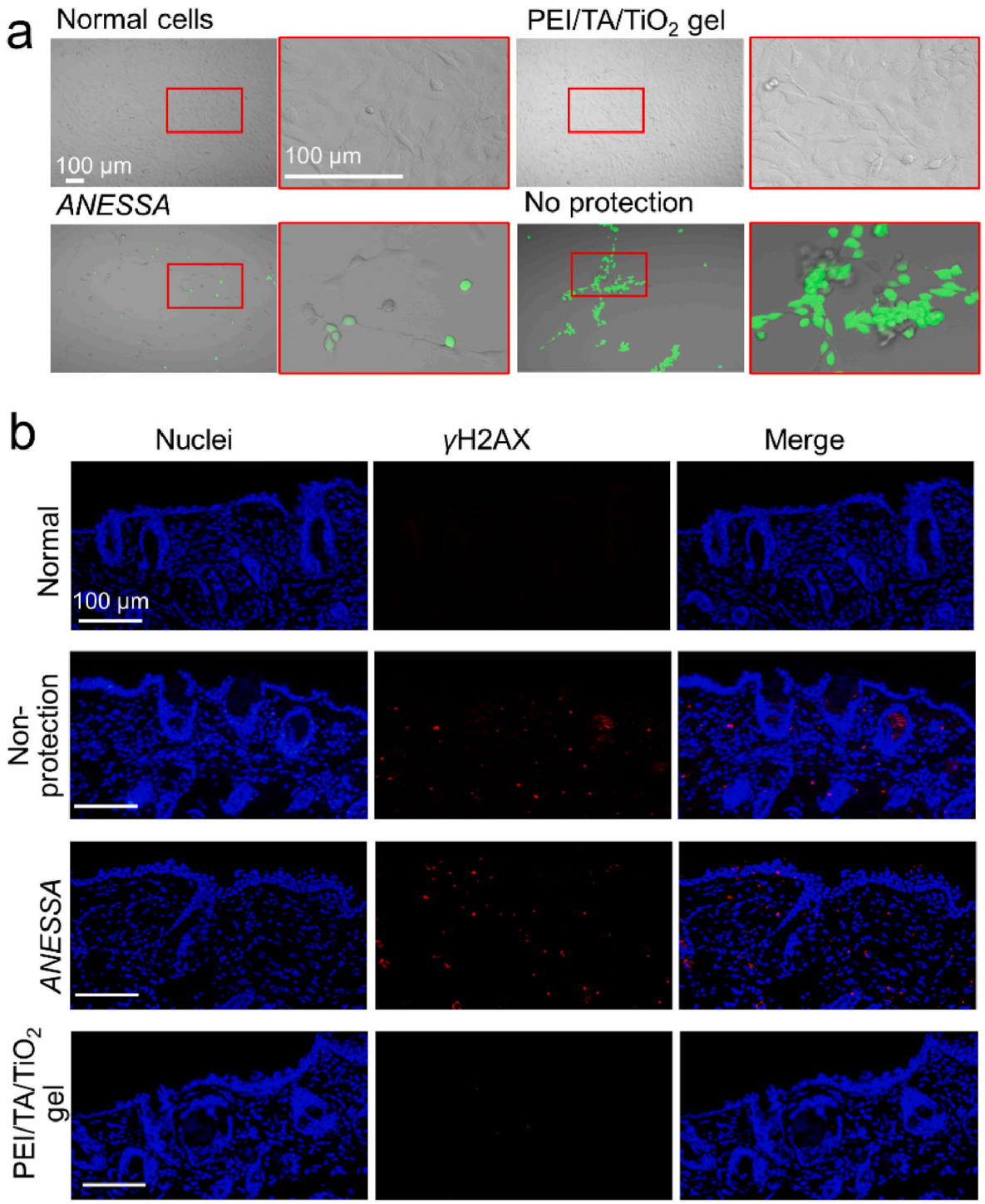

Fig. 6. (a) ROS generation images of 3T3 cells in different groups containing normal cells, cells protected with PEI/TA/TiO_2 hydrogel and *ANESSA*, and cells with non-protection. (b) γH2AX staining of the dorsal mouse skin of different groups including the normal group, non-protection group, *ANESSA* group, and PEI/TA/TiO_2 hydrogel group.

Methodology. **Kunyu Zhang:** Writing – review & editing. **Xin Zhao:** Writing – review & editing. **Gang Li:** Project administration, Funding acquisition. **Liming Bian:** Supervision, Project administration, Funding acquisition, Writing – review & editing.

Declaration of competing interest

The authors declare that they have no conflict of interest.

Acknowledgements

Xin Peng, Yuan Li and Menghui Liu contributed equally to this work. This work was financially supported by the National Key Research and Development Program (2022YFB3804403). This work was supported by the Collaborative Research Fund from the Research Grants Council of Hong Kong (Project No. C5044-21G). This work was supported by the Research Grants Council of the Hong Kong Special Administration Region (project no. GRF/14202920, GRF/14204618, GRF/14108720,

T13-402/17-N and AoE/M-402/20), Health@InnoHK program launched by Innovation Technology Commission of the Hong Kong SAR, P.R. China. This work was supported by This work was supported by National Natural Science Foundation of China (22205264).

Appendix A. Supplementary data

Supplementary data to this article can be found online at https://doi.org/10.1016/j.bioactmat.2023.07.016.

References

[1] F.P. Noonan, J.A. Recio, H. Takayama, P. Duray, M.R. Anver, W.L. Rush, E.C. De Fabo, G. Merlino, Neonatal sunburn and melanoma in mice, Nature 413 (6853) (2001) 271–272.
[2] Z. Corbyn, Prevention: lessons from a sunburnt country, Nature 515 (7527) (2014) S114–S116.
[3] E.R. Gonzaga, Role of UV light in photodamage, skin aging, and skin cancer, Am. J. Clin. Dermatol. 10 (1) (2009) 19–24.
[4] B. Diffey, P. Farr, Sunscreen protection against UVB, UVA and blue light: an *in vivo* and *in vitro* comparison, Br. J. Dermatol. 124 (3) (1991) 258–263.
[5] F.P. Gasparro, M. Mitchnick, J.F. Nash, A review of sunscreen safety and efficacy, Photochem. Photobiol. 68 (3) (1998) 243–256.
[6] D. Bhattacharjee, S. Preethi, A.B. Patil, V. Jain, A comparison of natural and synthetic sunscreen agents: a review, J. Int. Pharm. Res. 13 (1) (2021).
[7] N. Serpone, D. Dondi, A. Albini, Inorganic and organic UV filters: their role and efficacy in sunscreens and suncare products, Inorg. Chim. Acta. 360 (3) (2007) 794–802.
[8] U. Osterwalder, B. Herzog, Chemistry and Properties of Organic and Inorganic UV Filters, Clinical Guide to Sunscreens and Photoprotection, CRC Press2008, pp. 27-54.
[9] R. Dunford, A. Salinaro, L. Cai, N. Serpone, S. Horikoshi, H. Hidaka, J. Knowland, Chemical oxidation and DNA damage catalysed by inorganic sunscreen ingredients, FEBS Lett. 418 (1–2) (1997) 87–90.
[10] S. Butt, T. Christensen, Toxicity and phototoxicity of chemical sun filters, Radiat. Protect. Dosim. 91 (1–3) (2000) 283–286.
[11] S.L. Schneider, H.W. Lim, Review of environmental effects of oxybenzone and other sunscreen active ingredients, J. Am. Acad. Dermatol. 80 (1) (2019) 266–271.
[12] É.M. Nery, R.M. Martinez, M.V.R. Velasco, A.R. Baby, A short review of alternative ingredients and technologies of inorganic UV filters, J. Cosmet. Dermatol. 20 (4) (2021) 1061–1065.
[13] E.B. Manaia, R.C.K. Kaminski, M.A. Corrêa, L.A. Chiavacci, Inorganic UV filters, Braz. J. Pharm. Sci. 49 (2) (2013) 201–209.
[14] X. Fan, Y. Fang, W. Zhou, L. Yan, Y. Xu, H. Zhu, H. Liu, Mussel foot protein inspired tough tissue-selective underwater adhesive hydrogel, Mater. Horiz. 8 (3) (2021) 997–1007.
[15] X. Liu, L. Shi, X. Wan, B. Dai, M. Yang, Z. Gu, X. Shi, L. Jiang, S. Wang, A spider-silk-inspired wet adhesive with supercold tolerance, Adv. Mater. 33 (14) (2021), 2007301.
[16] C. Cui, W. Liu, Recent advances in wet adhesives: adhesion mechanism, design principle and applications, Prog. Polym. Sci. 116 (2021), 101388.
[17] C.Y. Cui, T.L. Wu, X.Y. Chen, Y. Liu, Y. Li, Z.Y. Xu, C.C. Fan, W.G. Liu, A Janus hydrogel wet adhesive for internal tissue repair and anti-postoperative adhesion, Adv. Funct. Mater. 30 (49) (2020).
[18] Y. Wang, E.J. Jeon, J. Lee, H. Hwang, S.W. Cho, H. Lee, A phenol-amine superglue inspired by insect sclerotization process, Adv. Mater. 32 (43) (2020), 202002118.
[19] R. Wang, X. Wang, Y. Zhan, Z. Xu, Z. Xu, X. Feng, S. Li, H. Xu, A dual network hydrogel sunscreen based on poly-γ-glutamic acid/tannic acid demonstrates excellent anti-UV, self-recovery, and skin-integration capacities, ACS Appl. Mater. Interfaces 11 (41) (2019) 37502–37512.
[20] C. Wang, D. Wang, T. Dai, P. Xu, P. Wu, Y. Zou, P. Yang, J. Hu, Y. Li, Y. Cheng, Skin pigmentation-inspired polydopamine sunscreens, Adv. Funct. Mater. 28 (33) (2018), 1802127.
[21] V.C. Prado, M.H.M. Sari, B.C. Borin, R. do Carmo Pinheiro, L. Cruz, A. Schuch, C. W. Nogueira, G. Zeni, Development of a nanotechnological-based hydrogel containing a novel benzofuroazepine compound in association with vitamin E: an in vitro biological safety and photoprotective hydrogel, Colloids Surf., B 199 (2021), 111555.
[22] Z. Tang, Y. Miao, J. Zhao, H. Xiao, M. Zhang, K. Liu, X. Zhang, L. Huang, L. Chen, H. Wu, Mussel-inspired biocompatible polydopamine/carboxymethyl cellulose/polyacrylic acid adhesive hydrogels with UV-shielding capacity, Cellulose 28 (3) (2021) 1527–1540.
[23] Y.-C. Lin, Y.-P. Fang, C.-F. Hung, H.-P. Yu, A. Alalaiwe, Z.-Y. Wu, J.-Y. Fang, Multifunctional TiO_2/SBA-15 mesoporous silica hybrids loaded with organic sunscreens for skin application: the role in photoprotection and pollutant adsorption with reduced sunscreen permeation, Colloids Surf., B 202 (2021), 111658.
[24] Y.-C. Lin, C.-F. Lin, A. Alalaiwe, P.-W. Wang, Y.-P. Fang, J.-Y. Fang, UV filter entrapment in mesoporous silica hydrogel for skin protection against UVA with minimization of percutaneous absorption, Eur. J. Pharmaceut. Sci. 122 (2018) 185–194.
[25] H. Wang, X. Yi, T. Liu, J. Liu, Q. Wu, Y. Ding, Z. Liu, Q. Wang, An integrally formed Janus hydrogel for robust wet-tissue adhesive and anti-postoperative adhesion, Adv. Mater. (2023), 202300394.
[26] S.J. Wu, H. Yuk, J. Wu, C.S. Nabzdyk, X. Zhao, A multifunctional origami patch for minimally invasive tissue sealing, Adv. Mater. 33 (11) (2021), 202007667.
[27] T. Xie, J. Ding, X. Han, H. Jia, Y. Yang, S. Liang, W. Wang, W. Liu, W. Wang, Wound dressing change facilitated by spraying zinc ions, Mater. Horiz. 7 (2) (2020) 605–614.
[28] X. Chen, H. Yuk, J. Wu, C.S. Nabzdyk, X. Zhao, Instant tough bioadhesive with triggerable benign detachment, P. Natl. Acad. Sci. USA 117 (27) (2020) 15497–15503.
[29] Y. He, Q. Li, P. Chen, Q. Duan, J. Zhan, X. Cai, L. Wang, H. Hou, X. Qiu, A smart adhesive Janus hydrogel for non-invasive cardiac repair and tissue adhesion prevention, Nat. Commun. 13 (1) (2022), 7666-7666.
[30] L. Xiong, M. Zhao, Y. Fan, S. Wang, Y. Yang, X. Li, D. Zhao, F. Zhang, Manganese oxide nanoclusters for skin photoprotection, ACS Appl. Bio Mater. 2 (9) (2019) 3974–3982.
[31] X. Peng, Y. Li, T. Li, Y. Li, Y. Deng, X. Xie, Y. Wang, G. Li, L. Bian, Coacervate-derived hydrogel with effective water repulsion and robust underwater bioadhesion promotes wound healing, Adv. Sci. 9 (31) (2022), 2203890.